

Aromaticity Reversal Induced by Vibrations in Cyclo[16]carbon

Igor Rončević,* Freddie J. Leslie,[§] Max Rossmannek,[§] Ivano Tavernelli, Leo Gross, and Harry L. Anderson



Cite This: <https://doi.org/10.1021/jacs.3c10207>



Read Online

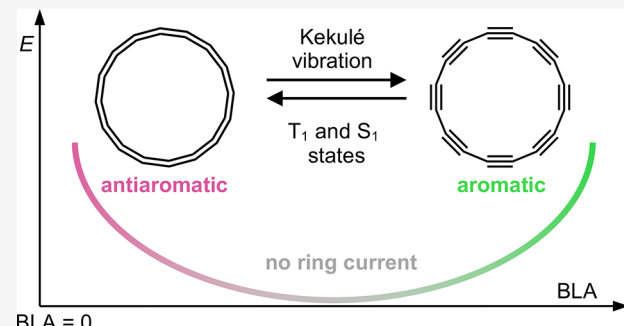
ACCESS |

Metrics & More

Article Recommendations

Supporting Information

ABSTRACT: Aromaticity is typically regarded as an intrinsic property of a molecule, correlated with electron delocalization, stability, and other properties. Small variations in the molecular geometry usually result in small changes in aromaticity, in line with Hammond's postulate. For example, introducing bond-length alternation in benzene and square cyclobutadiene by modulating the geometry along the Kekulé vibration gradually decreases the magnitude of their ring currents, making them less aromatic and less antiaromatic, respectively. A sign change in the ring current, corresponding to a reversal of aromaticity, typically requires a gross perturbation such as electronic excitation, addition or removal of two electrons, or a dramatic change in the molecular geometry. Here, we use multireference calculations to show how movement along the Kekulé vibration, which controls bond-length alternation, induces a sudden reversal in the ring current of cyclo[16]carbon, C₁₆. This reversal occurs when the two orthogonal π systems of C₁₆ sustain opposing currents. These results are rationalized by a Hückel model which includes bond-length alternation, and which is combined with a minimal model accounting for orbital contributions to the ring current. Finally, we successfully describe the electronic structure of C₁₆ with a “divide-and-conquer” approach suitable for execution on a quantum computer.



1. INTRODUCTION

Aromaticity is one of the most debated concepts in chemistry, and its definition has undergone several revisions over the last few decades.^{1–5} Today, the most commonly used criterion for aromaticity is magnetic,² equating the presence of a diatropic or paratropic ring current in an applied magnetic field with aromaticity or antiaromaticity, respectively. In molecules with several π systems, local and/or global currents may be present simultaneously,^{6,7} reinforcing or opposing each other. Aromaticity is a defining characteristic of a molecule, linked with reactivity, stability, HOMO–LUMO⁸ and singlet–triplet gaps,⁹ feasibility for singlet fission,¹⁰ diradical character,¹¹ wave function coherence,¹² and other properties.

Cyclo[N]carbons are all-carbon rings with two orthogonal π systems, usually with N electrons in each.¹³ In an analogy to annulenes, cyclocarbons with $N = 4n + 2$ carbon atoms can be classed as doubly aromatic (with both π systems sustaining a diatropic ring current), while $N = 4n$ cyclocarbons are expected to be doubly antiaromatic.^{14,15} Many cyclocarbons have been found in the gas phase, but only C₁₀,¹⁶ C₁₄,¹⁶ C₁₆,¹⁷ and C₁₈¹⁸ have been structurally characterized using scanning probe microscopy.

A recent on-surface investigation of C₁₆ revealed the presence of strong bond-length alternation (BLA) and confirmed that its ground state is doubly antiaromatic.¹⁷ Here, we investigate the variation of aromaticity with geometry in the two lowest singlets (S₀ and S₁), the lowest triplet (T₁)

and quintet (Q₁) state of C₁₆. Surprisingly, we find that the total ring current in the S₁ and T₁ states can be reversed from aromatic to antiaromatic by movement along the Kekulé vibration ($\sim 2300\text{ cm}^{-1}$), i.e., by changing the amount of bond-length alternation.¹⁹ These aromaticity reversals require a relatively small amount of energy, in contrast with previous reports which require a change in the electronic state,^{20–23} molecular charge^{24–26} or composition,^{27,28} or involve a high-lying transition state^{29,30} or a highly strained geometry.³¹ To our knowledge, the only comparable low-energy aromaticity reversal involves a conformational equilibrium between Hückel antiaromatic and Möbius aromatic conformers in a hexaphyrin derivative.^{32,33}

The simplicity and unique electronic structure of cyclo-carbons makes them an interesting testing ground for theoretical methods.¹³ Quantum algorithms, which strongly benefit from execution on a quantum computer, are a promising avenue for the further development of electronic structure methods. However, their execution on current quantum devices is limited by noise and coherence time.^{34,35}

Received: September 16, 2023

Revised: October 29, 2023

Accepted: October 31, 2023

Here, we exploit the orthogonality between the two π systems of C_{16} to effectively increase the active space of the quantum unitary coupled clusters singles doubles (q-UCCSD) method,³⁶ which we solve variationally.³⁷ This divide-and-conquer approach enables us to obtain highly accurate results that would otherwise not be feasible to compute using near-term quantum devices.

1.1. Ipsocentric Approach. Before discussing the electronic structure and ring current in C_{16} , we briefly summarize the rules for evaluating orbital contributions to magnetic properties in the ipsocentric approach, as developed by Steiner and Fowler:^{38–40}

1. The current density J induced by a magnetic field (which, when integrated over the ring, gives the ring current strength, usually measured in nA/T) can be expressed as a sum of spin-allowed transitions from occupied (ψ_s) to unoccupied (ψ_t) orbitals. The contribution of each transition (J_{st}) can be written as a sum of a diatropic term (J_{st}^{DIA}), which is associated with aromaticity, and a paratropic term (J_{st}^{PARA}) associated with antiaromaticity:

$$J = \sum_s \sum_t J_{st} = \sum_s \sum_t (J_{st}^{\text{DIA}} + J_{st}^{\text{PARA}}) \quad (1)$$

The diatropic current, which opposes the externally applied field, is taken to be positive ($J^{\text{DIA}} > 0$), while the paratropic current, which reinforces the external field, is taken to be negative ($J^{\text{PARA}} < 0$).

- 2 The diatropic (aromatic) contribution of a transition from ψ_s to ψ_t to the current density (J_{st}^{DIA}) is determined by the orbital energy difference $\Delta\epsilon_{st}$ and the translational matrix element M_{st}^T , which reflects the orbital coupling under the linear momentum operator \hat{p} (represented by T in Figure 1):³⁹

$$J_{st}^{\text{DIA}} \propto \frac{M_{st}^T}{\Delta\epsilon_{st}} = \frac{\langle \psi_t | \hat{p} | \psi_s \rangle}{\Delta\epsilon_{st}} \quad (2)$$

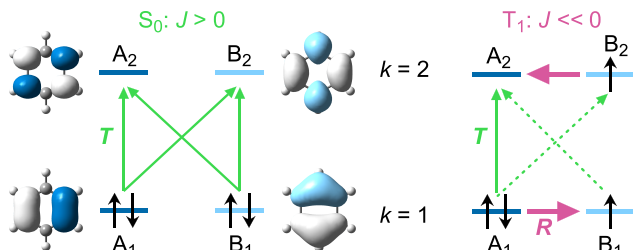
In general, M_{st}^T will be large for spatially similar orbitals differing in the number of nodal planes by one,³⁸ corresponding (in planar monocyclic molecules) to a change in the angular momentum k by one. For example, the purely diatropic ring current in benzene can wholly be attributed to translational transitions from $k = 1$ to $k = 2$ (Figure 1a left).⁴⁰

- 3 The contribution of an orbital pair to the paratropic current (J_{st}^{PARA}) is also modulated by $\Delta\epsilon_{st}$ and depends on the magnitude of the rotational matrix element M_{st}^R , which couples the orbitals under the angular momentum operator \hat{l} (represented by R in Figure 1):³⁹

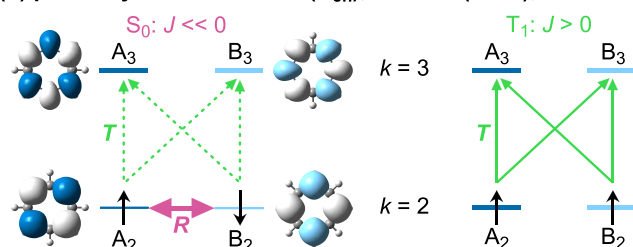
$$J_{st}^{\text{PARA}} \propto \frac{M_{st}^R}{\Delta\epsilon_{st}} = \frac{\langle \psi_t | \hat{l} | \psi_s \rangle}{\Delta\epsilon_{st}} \quad (3)$$

For planar monocyclic molecules without BLA, M_{st}^R will approach unity for orbital pairs related by a rotation, such as A_2 and B_2 in D_{8h} cyclooctatetraene (COT, Figure 1b; A and B correspond to sine and cosine density patterns). Such systems will have open-shell character^{21,41,42} and very large paratropic currents. Introducing BLA in planar COT (Figure 1c) lifts the degeneracy between A_2 and B_2 , producing a closed-shell

(a) benzene (D_{6h}); $4n + 2 \pi e^-$ ($n = 1$); BLA = 0



(b) planar cyclooctatetraene (D_{8h}); $4n \pi e^-$ ($n = 2$); BLA = 0



(c) planar cyclooctatetraene (D_{4h}); $4n \pi e^-$ ($n = 2$); BLA ≠ 0

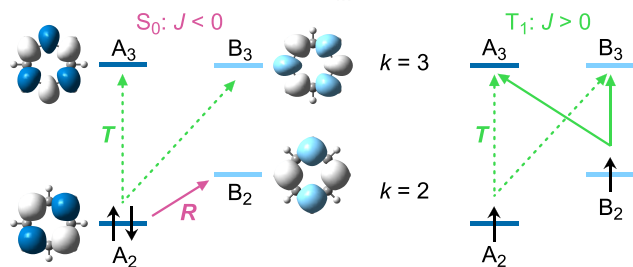


Figure 1. Translational (green, labeled T) and rotational (purple, labeled R) transitions in the lowest singlet (S_0 , left) and triplet (T_1 , right) state for (a) benzene, (b) planar COT with no BLA, and (c) planar COT with BLA. Full and dashed lines show relatively larger and smaller contributions to the ring current, respectively.

singlet, lowering the total energy and decreasing antiaromaticity.

- 4 From eqs 2 and 3, we can deduce that very few orbitals around the HOMO and LUMO will meaningfully contribute to the ring current. In aromatic annulenes, it is generally sufficient to consider only translational transitions with $\Delta k = 1$, i.e., HOMO \rightarrow LUMO. In antiaromatic annulenes, rotational transitions with $\Delta k = 0$ ($A_2 \leftrightarrow B_2$ in Figure 1b,c) are responsible for most of the ring current, with weak contributions from occupied orbitals below the HOMO.⁴⁰ We also note that this rule is valid only when the magnetic response is global, i.e., when the frontier orbitals are delocalized along the entire ring, which is valid up to $\sim C_{30}$ in the case of even-numbered cycloaromatics.²⁰

The ipsocentric approach provides an orbital-based rationalization of Baird's rule, which predicts an aromaticity reversal in the lowest triplet (T_1) state of annulenes compared to the S_0 ground state.⁴³ In benzene (Figure 1a right), promoting one electron to either A_2 or B_2 produces a very strong paratropic current, resulting in an aromaticity reversal in the T_1 (and S_1) excited states. On the other hand, in planar COT (Figure 1b,c) flipping an electron renders the rotational $A_2 \leftrightarrow B_2$ transitions forbidden, leading to a Baird aromatic T_1 state. Finally, the evaluation of aromaticity in the S_1 (and other excited states) is less straightforward due to a combination of diatropic and

paratropic contributions, in agreement with the experimental observation that Baird's rule is weaker for S_1 than for T_1 .⁴⁴

In the ground state (S_0) of C_{16} , the configuration of both π systems is similar to that in planar COT (Figure 1b,c). Flipping a single electron in C_{16} will result in a T_1 state with mixed aromaticity, where one π system will be Baird aromatic and the other will remain antiaromatic (norcorrole is a similar example⁴⁵). Flipping an electron in both π systems of C_{16} will result in a doubly Baird aromatic quintet (Q_1) state, as shown by Fowler.⁴⁶ We also investigate the S_1 state in which an electron moves from one π system to the other, resulting in a pair of oppositely charged doublets.

2. RESULTS AND DISCUSSION

To understand how the electronic structure and magnetic properties of C_{16} change with BLA (Figure 2a), we use three different approaches: (1) a tight-binding Hückel-Heilbronner model (HHM), described in the next section; (2) the complete active space self-consistent field (CASSCF) method; and (3) density functional theory (DFT). In CASSCF calculations, all orbitals in a predefined active space are optimized, and the wave function can be written as a linear combination of many configurations, all of which contribute to the final magnetic properties. In contrast, the DFT wave function is only a single determinant, with strictly defined orbital occupations.

2.1. Hückel–Heilbronner model. To gain more qualitative insight in the electronic structure of C_{16} , we employ a semiempirical HHM,⁴⁷ which extends the simple Hückel model by replacing the nearest neighbor interaction energy β with an alternating pattern of $\beta(1 + \delta)$ and $\beta(1 - \delta)$, as shown in Figure 2a:

$$\begin{bmatrix} \alpha & \beta(1 + \delta) & 0 & \cdots & 0 & \beta(1 - \delta) \\ \beta(1 + \delta) & \alpha & \beta(1 - \delta) & \cdots & 0 & 0 \\ 0 & \beta(1 - \delta) & \alpha & \cdots & 0 & 0 \\ \vdots & \vdots & \vdots & \ddots & \vdots & \vdots \\ 0 & 0 & 0 & \cdots & \alpha & \beta(1 + \delta) \\ \beta(1 - \delta) & 0 & 0 & \cdots & \beta(1 + \delta) & \alpha \end{bmatrix} \quad (4)$$

At $\delta = 0$, the HHM reduces to a simple Hückel model. At $0 < \delta < 1$, it describes a system in which the interaction between shorter bonds is given by $\beta(1 + \delta)$, while longer bonds are coupled by $\beta(1 - \delta)$, which was shown to be a good approximation by Stanger.⁴⁸ Previously, the HHM has been used to describe how frontier orbital energies of annulenes¹⁹ and azaboraheterocycles⁴⁹ change with BLA.

C_{16} has two π systems, with out-of-plane orbitals (interaction energy β'' , total energy E_π'') offset by γ relative to in-plane orbitals (interaction energy β' , total energy E_π'). Using HHM, we can find the π orbital energies of C_{16} by solving (4) twice, allowing for $\beta'' \neq \beta'$, as shown in Figure 2b. The total energy $E_{\text{TOT}}^{\text{HHM}}$ can be obtained by adding the sigma contribution $a_\sigma \delta^2$ (approximated as a parabola with the minimum at $\delta = 0$),⁴⁷ to the energies of the two π systems (E_π'' and E_π'):

$$E_{\text{TOT}}^{\text{HHM}} = a_\sigma \delta^2 + E_\pi''(\beta'', \delta) + E_\pi'(\beta', \delta, \gamma) \quad (5)$$

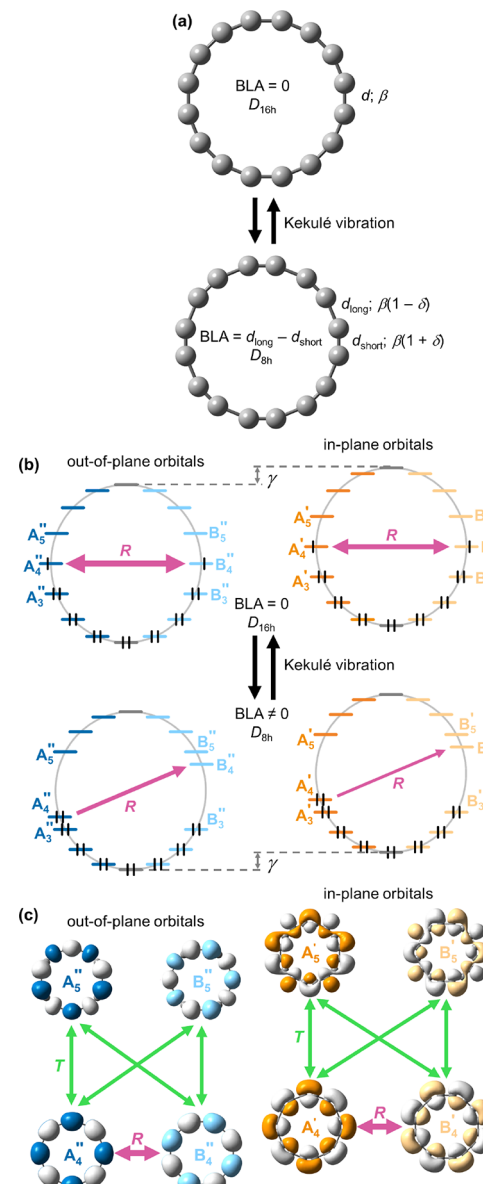


Figure 2. (a) BLA-inducing Kekulé vibration in C_{16} , with bond lengths d and nearest-neighbor couplings β denoted. Frost-Musulin diagrams (assuming $\beta'' = \beta'$) for C_{16} in the absence (top) and presence (bottom) of BLA, with the dominant paratropic contributions in the ground state shown in purple. Offset between the out-of-plane (blue) and in-plane (orange) π systems is denoted by γ . (b) Possible translational (T , green) and rotational (R , purple) transitions associated with $k = 4-5$ orbitals in low-lying electronic states of C_{16} .

In C_{16} without BLA, the frontier out-of-plane orbitals (A_4'' and B_4'' ; Figure 2b top) are energy degenerate and slightly ($\gamma = 0.1$ eV) lower in energy than their in-plane counterparts (A_4' and B_4'), resulting in an unstable double open shell singlet,¹⁷ in analogy to D_{4h} cyclobutadiene⁵⁰ or D_{8h} COT.^{21,23,42}

Introducing BLA lowers the energies of A_4'' and A_4' by $2\beta''\delta$ and $2\beta'\delta$ (and raises the energies of B_4'' and B_4' by the same value), resulting in a closed-shell doubly antiaromatic configuration. More generally, the HHM predicts that the introduction of BLA lowers the π energy of both $4n$ and $4n + 2$ systems, with the effect being smaller in $4n + 2$ than $4n$ systems with equal n and increasing with n (details in SI). Therefore, a

π -conjugated molecule will have no BLA if its σ contribution outweighs the π contribution, which usually occurs in $4n + 2$ molecules with small n (e.g., benzene), in agreement with Shaik's interpretation based on valence bond theory.⁵¹ A more rigorous discussion on the distortivity of π -conjugated systems can be found in refs 52, 53, and 54.

We extend the HHM to excited states by promoting electrons to unoccupied orbitals and adding a state-specific offset E_{xc} to the energy of the newly occupied orbitals, in order to account for orbital relaxation and exchange coupling; in state-averaged fashion, a_α , β'' , and β' are kept equal in all states (and at all values of BLA).

Two limitations of the HHM are that it is valid only at small BLA ($\delta \approx 0$) and that it only accounts for the changes in orbital energies, meaning that it cannot identify a possible switch from the global to a local current.

2.2. Minimal Ipsocentric Model for C₁₆. To provide a direct relation between aromaticity and orbital energies, we employ a minimal ipsocentric model in which matrix elements in eqs 2 and 3 are replaced by orbital-independent parameters, and only a few transitions are counted. In this approach, the total ring current of C₁₆ is calculated as the sum of its out-of-plane and in-plane components, which are given by

$$J'' = \sum_{s''} \sum_{t''} \left(\frac{c_{st}^{\text{DIA}} - c_{st}^{\text{PARA}}}{\Delta \epsilon_{s''t''}} \right) \quad (6)$$

$$J' = c' \sum_{s'} \sum_{t'} \left(\frac{c_{st}^{\text{DIA}} - c_{st}^{\text{PARA}}}{\Delta \epsilon_{s't'}} \right) \quad (7)$$

In eqs 6 and 7, c_{st}^{DIA} has a constant positive value for all transitions with $\Delta k = 1$ (e.g., A₄'' → A₅''), while c_{st}^{PARA} has a constant positive value for all $\Delta k = 0$ transitions; both are zero for all other transitions. The third parameter in the model, c' , relates the in-plane and the out-of-plane matrix elements (more generally, it relates the currents produced in different π systems by an orbital pair with the same $\Delta \epsilon_{st}$). c_{st}^{DIA} , c_{st}^{PARA} , and c' are assumed to be independent of BLA and electronic state; for a specific molecule, they reflect how much current is induced by a single transition between orbitals separated by one unit of energy.

Within this minimal model, only orbitals with $k = 3–5$ contribute to the ring current of C₁₆ (as only $\Delta k = 0$ and $\Delta k = 1$ transitions are counted). For simplicity, we will focus on transitions involving $k = 4$ and $k = 5$ orbitals shown in Figure 2c, as the diatropic contribution of $k = 3 \rightarrow k = 4$ transitions changes in the same manner as the contribution from $k = 4 \rightarrow k = 5$ transitions.

In principle, the three parameters c_{st}^{DIA} , c_{st}^{PARA} , and c' (or two, in the case of an annulene) can be obtained by only three (or two) calculations. In the next section, we use a more sophisticated approach based on CASSCF ring currents and HHM orbitals but note that similar values of c_{st}^{DIA} , c_{st}^{PARA} , and c' can be obtained by only three DFT calculations (see SI).

2.3. CASSCF and HMM results. We now investigate the variation of the ring current with BLA in the S₀, Q₁, T₁, and S₁ states of C₁₆ at a series of 11 D_{8h} geometries with different values of BLA. The considered geometries are interpolated between the ground-state minimum previously found by NEVPT2¹⁷ (BLA = 11.4 pm, ring radius $r = 3.33 \text{ \AA}$) and the minimum-energy D_{16h} geometry at the same level of theory (BLA = 0 pm, $r = 3.32 \text{ \AA}$); results for geometries extended to

BLA up to 16 pm, which roughly corresponds to the CASSCF minimum at $r = 3.32 \text{ \AA}$, are given in Figure 8.

CASSCF calculations include 12 electrons in 12 orbitals with $k = 3–5$ in the active space, capturing all $\Delta k = 0$ and $\Delta k = 1$ transitions. These CASSCF(12,12) energies (E_{CAS}) and ring currents (J_{CAS}), calculated from nucleus independent chemical shifts (NICS(2)_{zz}) are used to obtain the optimal parameters for the HHM and the minimal ipsocentric model (E_{HHM} , J_{HHM}). In both cases, J is expressed relative to the benzene ring current ($J_{\text{ref}} = 12 \text{ nA/T}$).

In the following section, different configurations are named according to the occupancies of their four $k = 4$ orbitals¹⁷ (Figure 3), e.g., S₀ at large BLA (Figure 2a bottom) can be

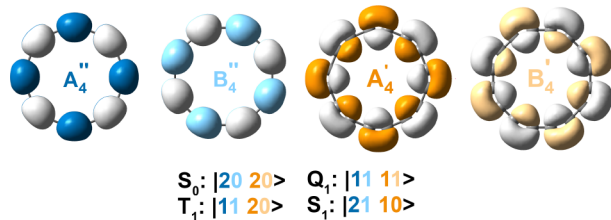


Figure 3. Most important configurations in the investigated electronic states of C₁₆.

written as |20 20>. For each electronic state, the magnetic couplings in the most relevant configuration are described. The effect of dynamic correlation is evaluated by comparing the CASSCF and QD-NEVPT2⁵⁵ wave function composition, as well as by density functional theory (DFT) calculations (ω B97XD/def2-TZVP, Figure S1 in SI).

2.4. S₀ State. In the ground state, the dominant configuration at virtually all nonzero BLA values is the doubly antiaromatic |20 20> (Figure 4a,d). In this configuration, A₄ orbitals in both π systems are doubly occupied and their B₄ counterparts are doubly unoccupied, leading to A₄'' → B₄'' and A₄' → B₄' rotational transitions (Figure 4b).

Decreasing BLA reduces the energy difference between A₄ and B₄, which rapidly increases antiaromaticity and electronic energy (Figure 4c; we define $E_{\text{rel}} = 0$ for BLA = 11.4 pm). Despite a strong multireference character at low BLA (Figure 4a), HHM reproduces the CASSCF results well (Figure 4c), with low mean absolute errors for energy MAE_E = 0.05 eV and ring current (MAE_J = 1.0).

There is a complete absence of the doubly aromatic |22 00> configuration, even at zero BLA, which is a consequence of a small separation γ between the two π systems.¹⁷ This is in contrast with single-reference methods and HHM, which incorrectly predict a |2200> ground state for the BLA = 0 configuration.

2.5. Q₁ State. The major configuration in the lowest quintet state is ⁵|11 11>, in which the four $k = 4$ orbitals are singly occupied by four same-spin electrons. This wave function composition remains largely unaffected by changes in BLA (Figure 5a). No rotational transitions are allowed, leading to double aromaticity (Figure 5b,d).⁴⁶

The Q₁ ring current does not change much (~10%) with BLA, as the increase in the energy of the A₄ orbitals is offset by a decrease in B₄ energies. At BLA = 0, the energy is minimized and the ring current is maximized (Figure 5c), which is a complete reversal of the result obtained for the doubly antiaromatic S₀ (cf. Figures 4c and 5c). A very similar result is obtained with DFT (Figure S1b).

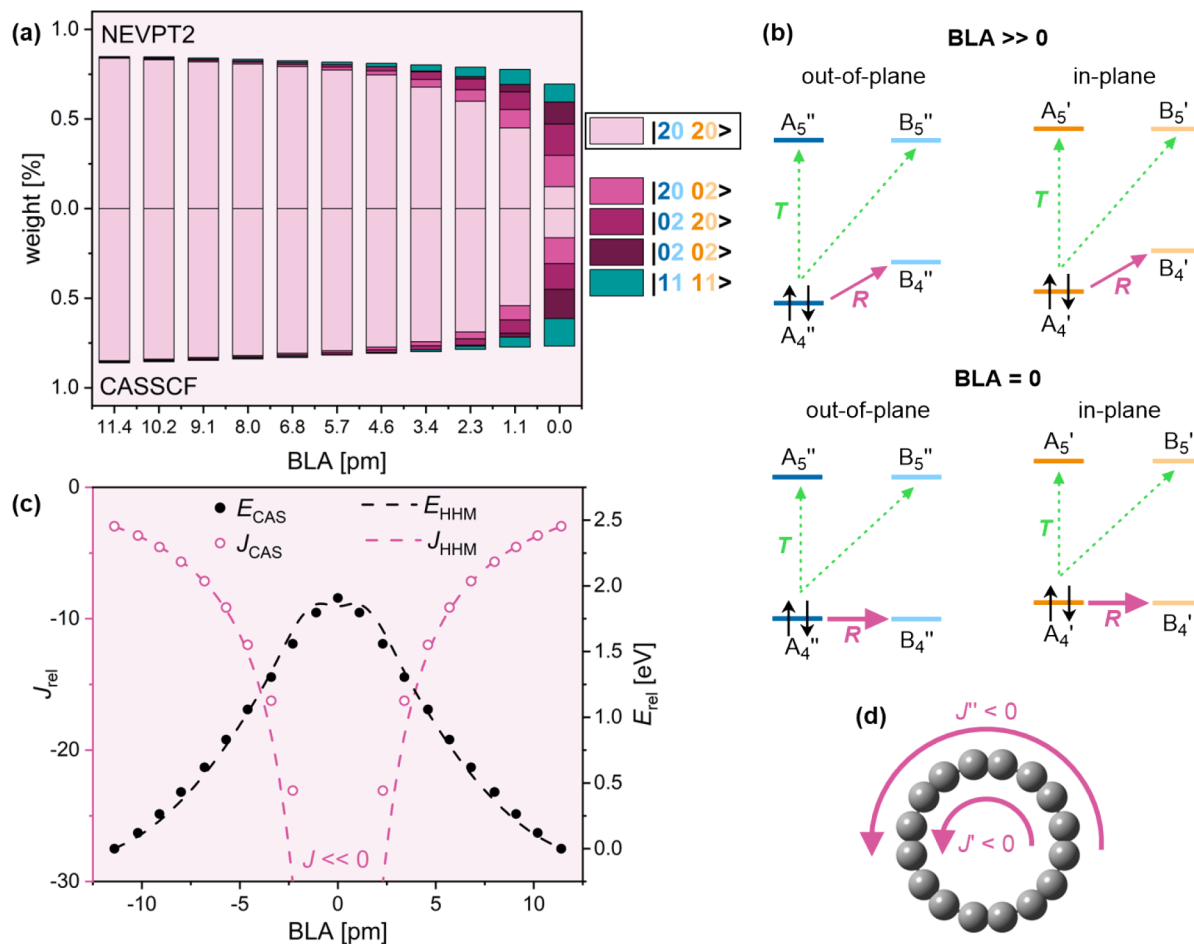


Figure 4. Aromaticity of C₁₆ in the ground (S₀) state. (a) Wave function composition at different BLA, as calculated by QD-NEVPT2 (top) and CASSCF (bottom). (b) Translational (green) and rotational (purple) transitions in $k = 4\text{--}5$ orbitals at large and zero BLA in the l20 20> configuration. Full and dashed lines show larger and smaller contributions to the ring current. (c) Total ring current and relative energy at different BLA calculated by CASSCF (circles) and the HHM (dashed lines). (d) In-plane (J') and out-of-plane (J'') contributions to the total ring current.

The HHM closely reproduces the electronic energies obtained by CASSCF (Figure 5c; MAE_E = 0.12 eV). The ring current fit is of similar accuracy to S₀ (MAE_J = 0.9), but it is limited by the inability of the minimal ipsocentric model to describe variation not driven by changes in orbital energies.

2.6. T₁ State. In a naïve single-reference picture, the lowest lying triplet state (T₁) might be obtained by changing the spin of a single electron in the S₀ l20 20> configuration. For example, flipping the spin of an electron in the out-of-plane π system results in the l11 20> configuration, which is predicted by both CASSCF and NEVPT2 to have the largest contribution to the multireference wave function (Figure 6a).

In l11 20>, the out-of-plane l11> π system produces a diatropic current, which does not depend much on the BLA (analogously to Q₁; Figure 6b left), while the paratropic current produced by the in-plane l20> π system strongly increases with decreasing BLA (analogously to S₀; Figure 6b). At this point, very small changes in energy (e.g., 70 meV in either direction, which corresponds to the expectation value of the value of position along the Kekulé vibration at 0 K) result in drastic changes in the ring current (from +0.9 to -2.3 relative to benzene). Unless a measurement with femtosecond resolution can be made, we will therefore observe an average paratropic current (around -1.4 relative to benzene); however,

this result illustrates the extreme variation in the magnetic susceptibility with small changes in energy and geometry.

The HHM qualitatively recovers the variation of energy with BLA, and reproduces the ring current changes with relatively high accuracy (Figure 6c; MAE_E = 0.09 eV; MAE_J = 0.3). The contribution of other notable configurations, such as l20 11> (in which an in-plane electron was flipped), is analogous to l11 20>, with a combination of paratropic and diatropic contributions. This is demonstrated by DFT, which predicts similar variation J with BLA for both cases (Figure S1c), in qualitative agreement with CASSCF.

2.7. S₁ State. Unlike all previously considered states, the first excited singlet (S₁) is antisymmetric with respect to the reflection of the molecular plane. This means it consists of configurations with an odd number of electrons in both π systems and can be described as a pair of doublets, with, e.g., 17 in-plane and 15 out-of-plane, or 15 in-plane and 17 out-of-plane electrons.

At nonzero BLA, both CASSCF and NEVPT2 predict l21 10>, which has 17 out-of-plane and 15 in-plane electrons, as the dominant configuration (Figure 7a). In l21 10>, a combination of rotational and translational transitions is present both π systems (Figure 7b), resulting in mixed aromaticity (Figure 7d). At large BLA (>9.1 pm), translational contributions are stronger, resulting in an overall diatropic

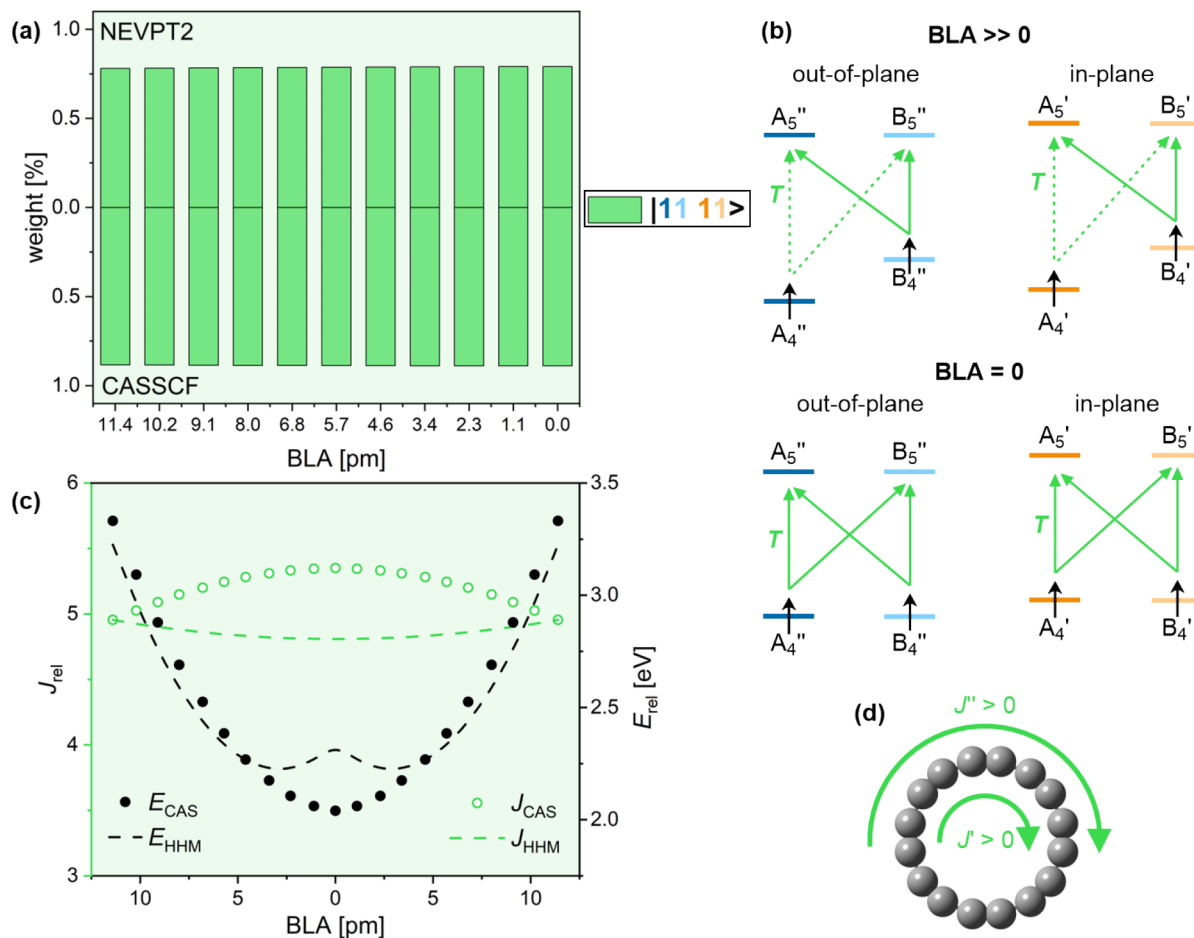


Figure 5. Aromaticity of C_{16} in the lowest quintet (Q_1) state. (a) Wave function composition at different BLA, as calculated by QD-NEVPT2 (top) and CASSCF (bottom). (b) Translational (green) and rotational (purple) transitions in $k = 4\text{--}5$ orbitals at large and zero BLA in the $|11\ 11\rangle$ configuration. Full and dashed lines show larger and smaller contributions to the ring current. (c) Total ring current and relative energy at different BLA calculated by CASSCF (circles) and the HHM (dashed lines). (d) In-plane (J') and out-of-plane (J'') contributions to the total ring current.

current. At smaller (<9.1 pm) BLA, the energy difference between A_4 and B_4 orbitals sufficiently shrinks to induce a reversal of the ring current (Figure 7c).

The similarity in the variation of energy and ring current in the T_1 (Figure 6) and S_1 (Figure 7) states can be rationalized by noting that their energies are approximately related by $E_{S1} = E_{T1} + \gamma - E_{\text{EX}}$ where γ is the offset between the in-plane and out-of-plane orbitals and E_{EX} is the exchange interaction. Analogously, ring currents in T_1 and S_1 are similar because the number of diatropic and paratropic transitions in both is equal (cf. Figures 6b and 7b). At BLA = 9.1, the ring current in S_1 is slightly more sensitive to small changes in energy, with a 70 meV variation in either direction changing J from +0.8 to −3.5.

The HHM fit to CASSCF energies and ring current is comparable to that of other states ($\text{MAE}_E = 0.06$ eV; $\text{MAE}_J = 0.6$), indicating that the HHM and the minimal ipso-centric approach can be extended to excited states.

2.8. Qualitative Modeling. The state-averaged HHM is successful in describing the variation of energy with BLA in the four lowest-lying electronic states of C_{16} (Figure 8a), with $\text{MAE}_E = 0.09$ eV. The HHM orbital separation γ is 0.2 eV, in good agreement with the $\gamma = 0.1$ eV value previously found by DFT.¹⁷ We also obtain a ∼38% stronger Hückel coupling between the out-of-plane ($\beta'' = 6.1$ eV) than the in-plane ($\beta' = 4.4$ eV) orbitals, indicating stronger overlap in the out-of-plane π system.

The frontier orbital ipso-centric approach accurately reproduces the aromaticity switching predicted by CASSCF, remaining remarkably robust through a large range of ring current strengths (Figure 8b), with a mean relative error of 11.9%. Its success validates the approximation that variation in the magnetic response can be recovered purely through the change in frontier orbital energies. The coupling constants we obtain are $c^{\text{DIA}} = 6.05$ J_{ref}/eV and $c^{\text{PARA}} = 8.05$ J_{ref}/eV , providing a simple, direct link between orbital energy and aromaticity through eqs 6 and 7. In agreement with previous work,^{20,46,56} our minimal ipso-centric approach finds a weaker magnetic coupling in the in-plane π system ($c' = 0.55$) relative to the out-of-plane system. Further details on the HHM and the minimal ipso-centric approach are given in the SI.

While we have only focused on the effect of BLA, aromaticity reversals may occur with any distortion that causes a stronger response in the orbital energies than in their spatial overlap. For example, bond-angle alternation (BAA) could be described by adding a $\beta_{\text{BAA}}(1 \pm \delta_{\text{BAA}})$ term to the in-plane π system. In cases where no significant open-shell character is present, the minimal ipso-centric approach could employ orbital energies calculated by DFT, making the calculation of coupling constants that relate aromaticity and frontier orbital energy very simple.

The addition of dynamic correlation does not seem to have a significant effect on the ring currents: DFT also predicts an

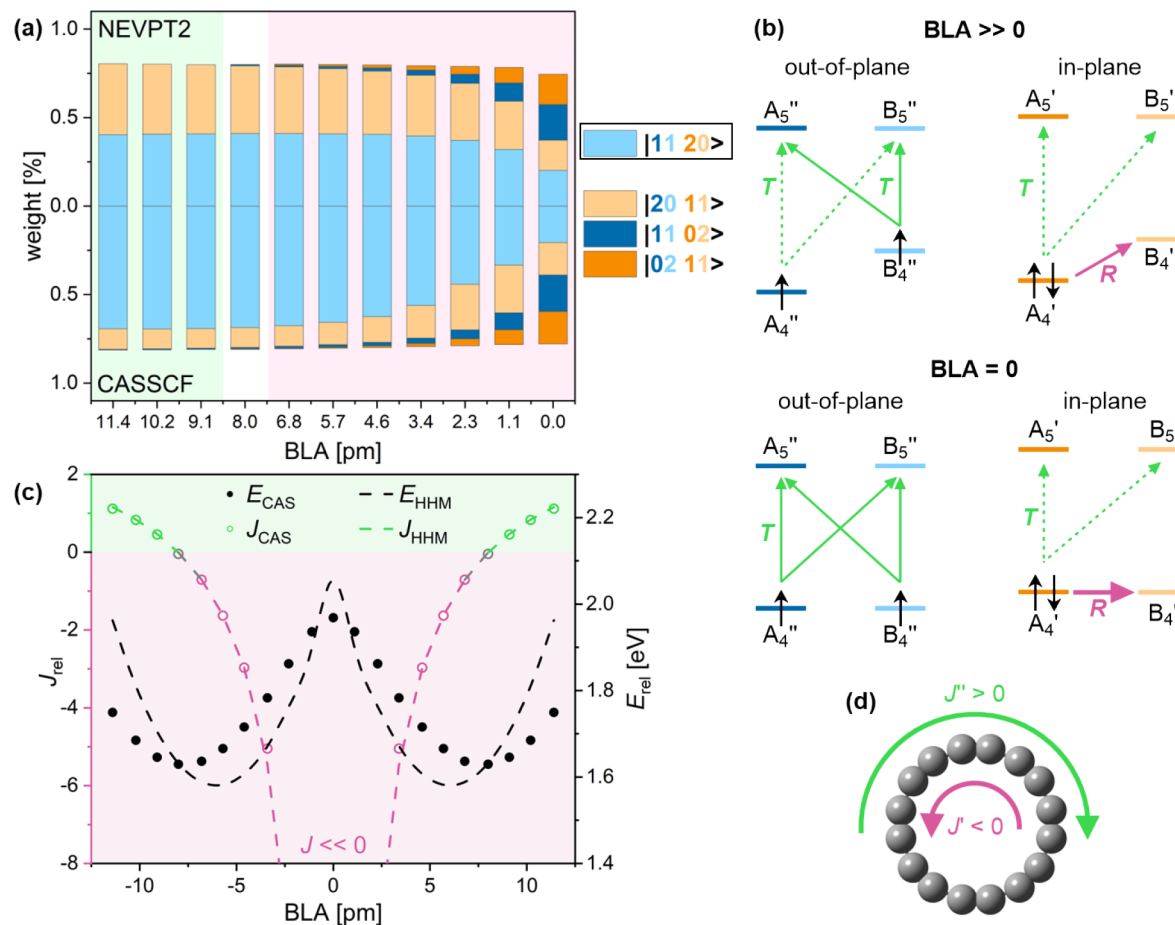


Figure 6. Aromaticity of C_{16} in the lowest triplet (T_1) state. (a) Wave function composition at different BLA, as calculated by QD-NEVPT2 (top) and CASSCF (bottom). (b) Translational (green) and rotational (purple) transitions in $k = 4\text{--}5$ orbitals at large and zero BLA in the $|11\ 20\rangle$ configuration. Full and dashed lines show larger and smaller contributions to the ring current. (c) Total ring current and relative energy at different BLA calculated by CASSCF (circles) and the HHM (dashed lines). (d) In-plane (J') and out-of-plane (J'') contributions to the total ring current.

aromaticity reversal in T_1 (Figure S1c), and perturbatively including coupling with unoccupied orbitals outside the active space (QD-NEVPT2) does not significantly change the composition (Figures 3a–6a) of the CASSCF wave function. This is in agreement with previous work comparing the performance of HF and DFT, which concluded that the computed current depends more strongly on the used geometry than on the level of theory.^{57,58}

2.9. Divide-and-Conquer Approach. Due to their orthogonality, the two π systems in cyclocarbons are usually considered separately.^{20,46,56} This suggests that one could approximate a 12,12 active space, which is used throughout this work, with a combination of in-plane and out-of-plane 6,6 active spaces. Here, we compute the energy of the two 6,6 subspaces (E'_{qUCCSD} and E''_{qUCCSD}) using the q-UCCSD* method, which includes all single and double excitations between all spin-orbitals in the active space (further details are given in the SI). The total energy is calculated according to

$$E_{\text{qUCCSD}}^{\text{total}} = E_{\text{inactive}(12,12)} + E'_{\text{qUCCSD}(6,6)} + E''_{\text{qUCCSD}(6,6)} \quad (8)$$

where $E_{\text{inactive}(12,12)}$ is the complete active space configuration interaction inactive energy, which can be obtained efficiently without solving the entire active space. It should be noted that in each of the two q-UCCSD(6,6) calculations, the correlated π -system feels the static orbitals of the noncorrelated π -system,

i.e., the two π -system systems remain coupled at a mean-field level.

In the S_0 state, this divide-and-conquer q-UCCSD approach works well for a wide range of nonzero BLA (Figure 9, MAE = 0.16 eV relative to CASSCF), producing results very similar to those of canonical CCSD and CCSD(T) methods. Around zero BLA, both q-UCCSD and canonical coupled clusters are limited by the poor quality of the underlying HF determinant, although q-UCCSD appears to be more robust in case of BLA ≈ 1 pm. In these cases, the performance of q-UCCSD may be further improved by starting from a better reference (e.g., CASSCF) or by using a flavor which includes orbital optimization.⁵⁹ q-UCCSD calculations for the T_1 and Q_1 states are of similar quality to S_0 (see the SI), illustrating a way for applying the q-UCCSD method to systems with many strongly correlated electrons (other possible use cases may be a complex with two weakly coupled transition metals, or a dye with two chromophores connected with sigma bonds).

3. CONCLUSIONS

Using CASSCF, qualitative modeling, and DFT, we have demonstrated that the ring current in C_{16} can be reversed by small changes in BLA. This reversal of aromaticity (according to the ring-current criterion²) is unique as it is not associated by any notable change in the electronic structure, but only with a small change in energy. It occurs in electronic states

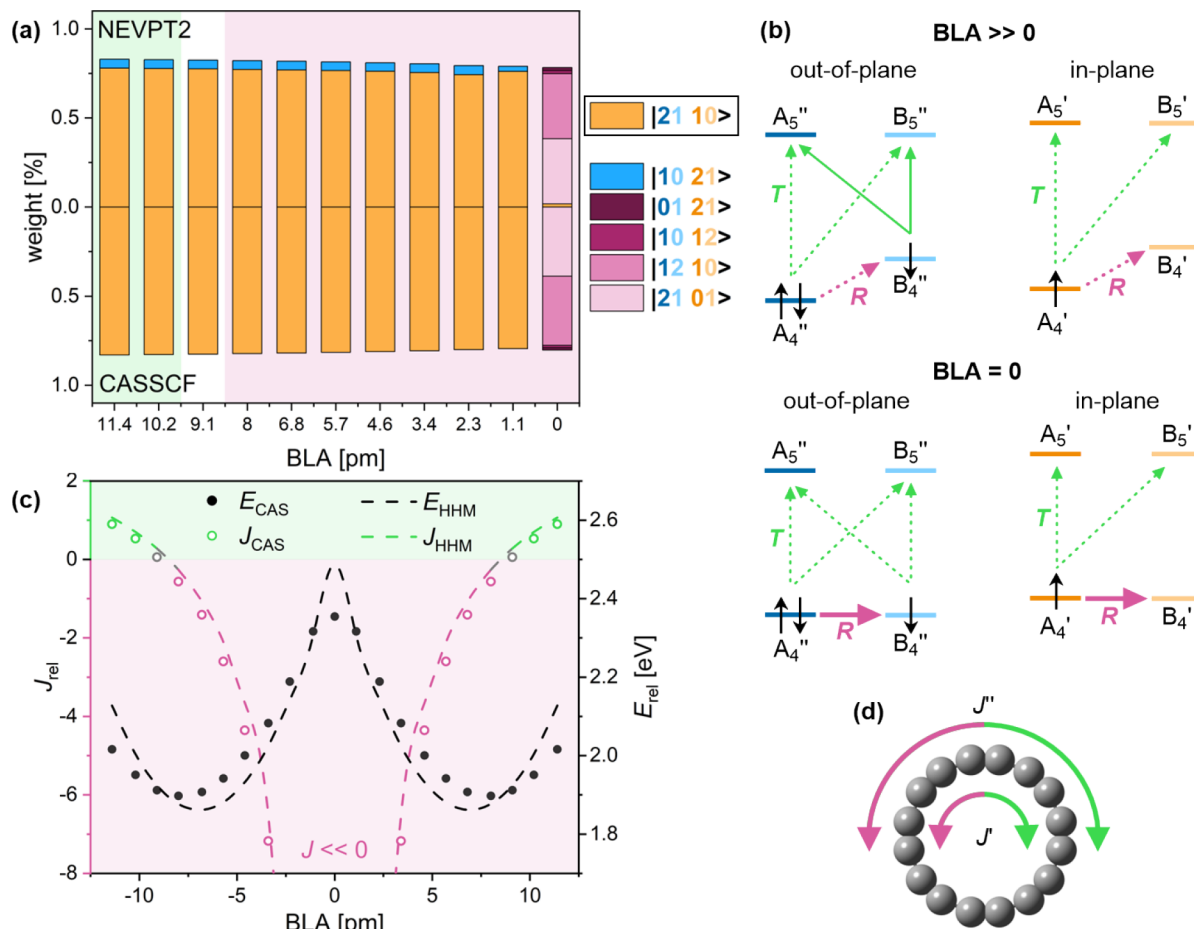


Figure 7. Aromaticity of C_{16} in the first excited singlet (S_1) state. (a) Wave function composition at different BLA, as calculated by QD-NEVPT2 (top) and CASSCF (bottom). (b) Translational (green) and rotational (purple) transitions in $k = 4-5$ orbitals at large and zero BLA in the $|21\ 10\rangle$ configuration. Full and dashed lines show larger and smaller contributions to the ring current. (c) Total ring current and relative energy at different BLA calculated by CASSCF (circles) and the HHM (dashed lines). (d) In-plane (J') and out-of-plane (J'') contributions to the total ring current.

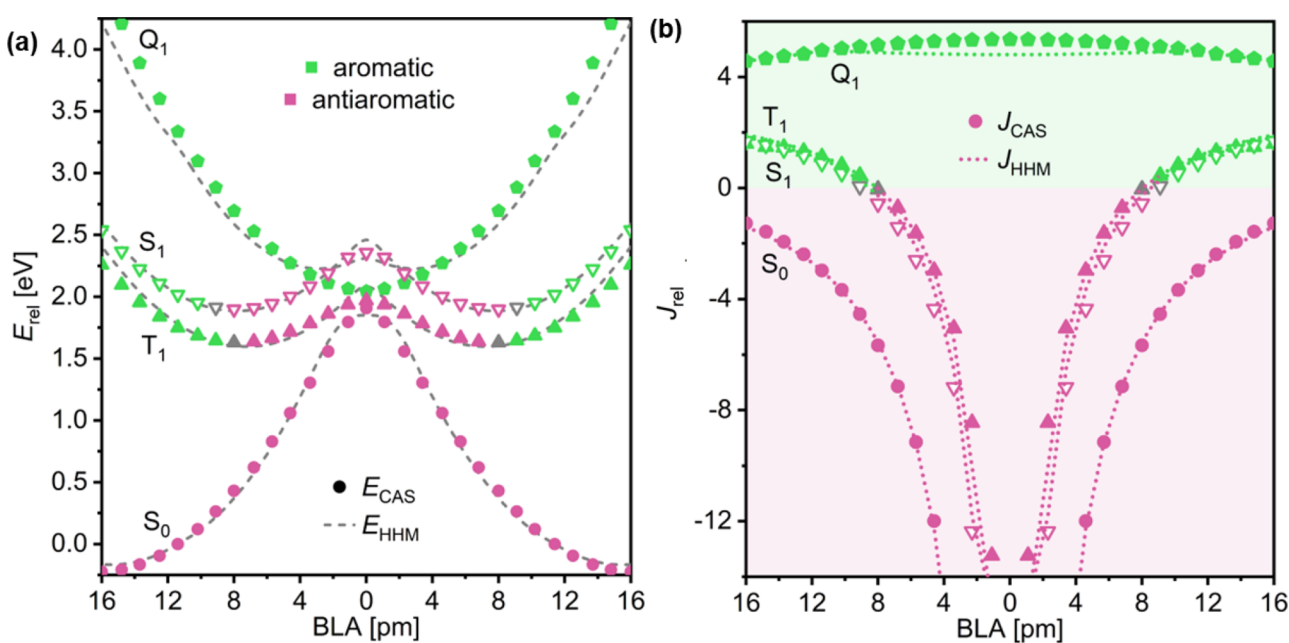


Figure 8. Comparison between (a) energies and (b) ring current strengths (b) predicted by CASSCF (large symbols) and the HHM (dotted lines). Circles correspond to the S_0 state, hollow triangles correspond to S_1 , full triangles correspond to T_1 , and pentagons correspond to Q_1 . Aromatic and antiaromatic ring currents are shown in green and purple, respectively.

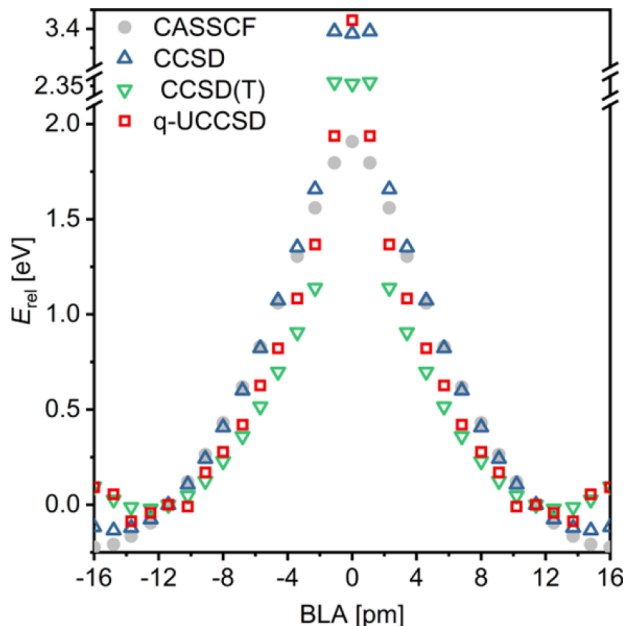


Figure 9. Energies of the S₀ state C₁₆ at different amounts of BLA calculated using CASSCF (gray circles), CCSD (blue hollow triangles), CCSD(T) (green hollow triangles), and divide-and-conquer q-UCCSD (red rectangles), all obtained with the cc-pVQZ basis set. Note the two breaks on the y axis.

Table 1. Ring Current of C₁₆ in Low-Living Electronic States at Different Amounts of Bond-Length Alteration

state	electronic structure	net ring current	
		BLA ≈ 0	BLA ≈ 0
S ₀	doubly antiaromatic	paratropic	paratropic
Q ₁	doubly Baird aromatic	diatropic	diatropic
T ₁	Baird aromatic + antiaromatic	diatropic	paratropic
S ₁	doubly mixed	diatropic	paratropic

displaying mixed aromaticity, which can be characterized by the presence of both diatropic and paratropic currents (Table 1).

The Hückel–Heilbronner tight-binding model captures the essence of the electronic structure of C₁₆, qualitatively reproducing the variation of energy obtained by much more complex methods (CASSCF and range-separated DFT). Magnetic couplings between the C₁₆ orbitals are successfully described by using a minimal ipso-centric model. This model provides a direct link between aromaticity and orbital energy, thus offering a simple avenue for rationalizing commonly observed correlations between aromaticity and various molecular properties.^{8,9,10,11}

Aromaticity reversals may also be interpreted in terms of antiaromaticity relief.^{30,60} The doubly aromatic Q₁ state adopts a BLA = 0 geometry, which maximizes its aromaticity, while the doubly antiaromatic S₀ minimizes its antiaromaticity by increasing BLA as much as the σ system allows. The mixed aromatic T₁ and S₁ states have approximately nonaromatic D_{8h} minima, revealing their aromatic and antiaromatic nature by movement along one and the other directions of the Kekulé vibration.

In any system with more than one π pathway, the ring currents produced by individual circuits may be opposed, leading to a possibility of aromaticity reversals of the type

discussed here. More generally, we can expect the behavior of such “mixed aromatic” systems to be very sensitive to changes in geometry.

We also demonstrate that the applicability of quantum algorithms such as q-UCCSD can be improved by partitioning the active space and calculating the correlation energy of each subspace separately. In the case of C₁₆, this divide-and-conquer approach is particularly successful, approaching the accuracy of fully self-consistent multireference calculations. Finally, as quantum devices have direct access to the wave function, it is straightforward to compute the expectation value of any observable. This suggests that the ipso-centric approach could be combined with virtually any quantum ansatz.

ASSOCIATED CONTENT

Supporting Information

The Supporting Information is available free of charge at <https://pubs.acs.org/doi/10.1021/jacs.3c10207>.

Molecular geometries, DFT results for the S₀, T₁, and Q₁ states, and MATLAB code used for the HHM ([PDF](#))

AUTHOR INFORMATION

Corresponding Author

Igor Rončević – Department of Chemistry, Oxford University, Chemistry Research Laboratory, Oxford OX1 3TA, United Kingdom; orcid.org/0000-0003-2175-8059; Email: igor.roncevic@chem.ox.ac.uk

Authors

Freddie J. Leslie – Department of Chemistry, Oxford University, Chemistry Research Laboratory, Oxford OX1 3TA, United Kingdom

Max Rossmannek – IBM Research Europe – Zurich, Rüschlikon 8803, Switzerland; orcid.org/0000-0003-1725-9345

Ivano Tavernelli – IBM Research Europe – Zurich, Rüschlikon 8803, Switzerland; orcid.org/0000-0001-5690-1981

Leo Gross – IBM Research Europe – Zurich, Rüschlikon 8803, Switzerland; orcid.org/0000-0002-5337-4159

Harry L. Anderson – Department of Chemistry, Oxford University, Chemistry Research Laboratory, Oxford OX1 3TA, United Kingdom; orcid.org/0000-0002-1801-8132

Complete contact information is available at: <https://pubs.acs.org/10.1021/jacs.3c10207>

Author Contributions

[§]These authors contributed equally.

Notes

The authors declare no competing financial interest.

ACKNOWLEDGMENTS

We thank David Tew, Shantanu Mishra, and Florian Albrecht for discussions. This work was supported by the ERC (grant 885606 ARO-MAT and grant 951519 MolDAM) and the European Commission (MSCA project 101064401 ElDelPath). Computational resources were provided by the Cirrus UK National Tier-2 HPC Service at EPCC (<http://www.cirrus.ac.uk>) funded by the University of Edinburgh and EPSRC (EP/P020267/1), as well as the Ministry of Education, Youth and Sports of the Czech Republic through the e-INFRA CZ (ID: 90140).

■ REFERENCES

- (1) Merino, G.; Solà, M.; Fernández, I.; Foroutan-Nejad, C.; Lazzaretti, P.; Frenking, G.; Anderson, H. L.; Sundholm, D.; Cossío, F. P.; Petrukhina, M. A.; et al. Aromaticity: Quo vadis. *Chem. Sci.* **2023**, *14*, 5569–5576.
- (2) Gershoni-Poranne, R.; Stanger, A. Magnetic criteria of aromaticity. *Chem. Soc. Rev.* **2015**, *44*, 6597–6615.
- (3) Schleyer, P. v. R. Introduction: Aromaticity. *Chem. Rev.* **2001**, *101*, 1115–1118.
- (4) Martín, N.; Scott, L. T. Challenges in aromaticity: 150 years after Kekulé's benzene. *Chem. Soc. Rev.* **2015**, *44*, 6397–6400.
- (5) Merino, G.; Solà, M. Celebrating the 150th anniversary of the kekulé benzene structure. *Phys. Chem. Chem. Phys.* **2016**, *18*, 11587–11588.
- (6) Bradley, D.; Jirásek, M.; Anderson, H. L.; Peeks, M. D. Disentangling global and local ring currents. *Chem. Sci.* **2023**, *14*, 1762–1768.
- (7) Stanger, A.; Monaco, G.; Zanasi, R. NICS-XY-scan predictions of local, semi-global, and global ring currents in annulated pentalene and s-indacene cores compared to first-principles current density maps. *ChemPhysChem* **2020**, *21*, 65–82.
- (8) Gershoni-Poranne, R.; Rahalkar, A. P.; Stanger, A. The predictive power of aromaticity: Quantitative correlation between aromaticity and ionization potentials and HOMO–LUMO gaps in oligomers of benzene, pyrrole, furan, and thiophene. *Phys. Chem. Chem. Phys.* **2018**, *20*, 14808–14817.
- (9) Frederickson, C. K.; Rose, B. D.; Haley, M. M. Explorations of the indenofluorenes and expanded quinoidal analogues. *Acc. Chem. Res.* **2017**, *50*, 977–987.
- (10) Stanger, A. Singlet fission and aromaticity. *J. Phys. Chem. A* **2022**, *126*, 8049–8057.
- (11) Xin, S.; Han, Y.; Fan, W.; Wang, X.; Ni, Y.; Wu, J. Enhanced aromaticity and open-shell diradical character in the dianions of 9-fluorenylidene-substituted expanded radialenes. *Angew. Chem., Int. Ed.* **2022**, *61*, No. e202209448.
- (12) Jirásek, M.; Anderson, H. L.; Peeks, M. D. From macrocycles to quantum rings: Does aromaticity have a size limit? *Acc. Chem. Res.* **2021**, *54*, 3241–3251.
- (13) Anderson, H. L.; Patrick, C. W.; Scriven, L. M.; Woltering, S. L. A short history of cyclocarbons. *Bull. Chem. Soc. Jpn.* **2021**, *94*, 798–811.
- (14) Baryshnikov, G. V.; Valiev, R. R.; Nasibullin, R. T.; Sundholm, D.; Kurten, T.; Ågren, H. Aromaticity of even-number cyclo[n]-carbons ($n = 6–100$). *J. Phys. Chem. A* **2020**, *124*, 10849–10855.
- (15) Baryshnikov, G. V.; Valiev, R. R.; Kuklin, A. V.; Sundholm, D.; Ågren, H. Cyclo[18]carbon: Insight into electronic structure, aromaticity, and surface coupling. *J. Phys. Chem. Lett.* **2019**, *10*, 6701–6705.
- (16) Sun, L.; Zheng, W.; Gao, W.; Kang, F.; Zhao, M.; Xu, W. Aromatic annular carbon allotropes: Cumulenic cyclo[10]carbon and Peierls-transition-intermediate cyclo[14]carbon. Research Square, 2023, DOI: [DOI: 10.21203/rs.3.rs-2616838/v2](https://doi.org/10.21203/rs.3.rs-2616838/v2).
- (17) Gao, Y.; Albrecht, F.; Rončević, I.; Ettedgui, I.; Kumar, P.; Scriven, L. M.; Christensen, K. E.; Mishra, S.; Righetti, L.; Rossmannek, M.; Tavernelli, I.; Anderson, H. L.; Gross, L. On-surface synthesis of a doubly anti-aromatic carbon allotrope *Nature* **2023** DOI: [10.1038/s41586-023-06566-8](https://doi.org/10.1038/s41586-023-06566-8).
- (18) Kaiser, K.; Scriven, L. M.; Schulz, F.; Gawel, P.; Gross, L.; Anderson, H. L. An sp-hybridized molecular carbon allotrope, cyclo[18]carbon. *Science* **2019**, *365*, 1299–1301.
- (19) Bean, D. E.; Fowler, P. W. Effect on ring current of the kekulé vibration in aromatic and antiaromatic rings. *J. Phys. Chem. A* **2011**, *115*, 13649–13656.
- (20) Baryshnikov, G. V.; Valiev, R. R.; Valiulina, L. I.; Kurtsevich, A. E.; Kurtén, T.; Sundholm, D.; Pittelkow, M.; Zhang, J.; Ågren, H. Odd-number cyclo[n]carbons sustaining alternating aromaticity. *J. Phys. Chem. A* **2022**, *126*, 2445–2452.
- (21) Karadakov, P. B. Aromaticity and antiaromaticity in the low-lying electronic states of cyclooctatetraene. *J. Phys. Chem. A* **2008**, *112*, 12707–12713.
- (22) Karadakov, P. B.; Di, M.; Cooper, D. L. Excited-state aromaticity reversals in möbius annulenes. *J. Phys. Chem. A* **2020**, *124*, 9611–9616.
- (23) Karadakov, P. B.; Preston, N. Aromaticity reversals and their effect on bonding in the low-lying electronic states of cyclooctatetraene. *Phys. Chem. Chem. Phys.* **2021**, *23*, 24750–24756.
- (24) Rickhaus, M.; Jirásek, M.; Tejerina, L.; Gotfredsen, H.; Peeks, M. D.; Haver, R.; Jiang, H.-W.; Claridge, T. D. W.; Anderson, H. L. Global aromaticity at the nanoscale. *Nat. Chem.* **2020**, *12*, 236–241.
- (25) Peeks, M. D.; Jirásek, M.; Claridge, T. D. W.; Anderson, H. L. Global aromaticity and antiaromaticity in porphyrin nanoring anions. *Angew. Chem., Int. Ed.* **2019**, *58*, 15717–15720.
- (26) Sokolov, A. Y.; Magers, D. B.; Wu, J. I.; Allen, W. D.; Schleyer, P. V. R.; Schaefer, H. F. III. Free cyclooctatetraene dianion: Planarity, aromaticity, and theoretical challenges. *J. Chem. Theory Comput.* **2013**, *9*, 4436–4443.
- (27) Jiang, Y.; Wu, Y.; Deng, J.; Wang, Z. Antiaromaticity–aromaticity transition of cyclo[16]carbon upon metal encapsulation. *Phys. Chem. Chem. Phys.* **2021**, *23*, 8817–8824.
- (28) Li, S.; Sun, Y.; Li, X.; Smaga, O.; Koniarz, S.; Pawlicki, M.; Chmielewski, P. J. Oxidative insertion of amines into conjugated macrocycles: Transformation of antiaromatic norcorrole into aromatic azacorrole. *Chem. Commun.* **2023**, *59*, 3739–3742.
- (29) Gibson, C. M.; Havenith, R. W. A.; Fowler, P. W.; Jenneskens, L. W. Planar homotropenylum cation: A transition state with reversed aromaticity. *J. Org. Chem.* **2015**, *80*, 1395–1401.
- (30) Slanina, T.; Ayub, R.; Toldo, J.; Sundell, J.; Rabten, W.; Nicaso, M.; Alabugin, I.; Fdez; Galván, I.; Gupta, A. K.; Lindh, R.; et al. Impact of excited-state antiaromaticity relief in a fundamental benzene photoreaction leading to substituted bicyclo[3.1.0]hexenes. *J. Am. Chem. Soc.* **2020**, *142*, 10942–10954.
- (31) Saha, P. K.; Mallick, A.; Turley, A. T.; Bismillah, A. N.; Danos, A.; Monkman, A. P.; Avestro, A.-J.; Yufit, D. S.; McGonigal, P. R. Rupturing aromaticity by periphery overcrowding. *Nat. Chem.* **2023**, *15*, 516–525.
- (32) Sankar, J.; Mori, S.; Saito, S.; Rath, H.; Suzuki, M.; Inokuma, Y.; Shinokubo, H.; Suk Kim, K.; Yoon, Z. S.; Shin, J.-Y.; et al. Unambiguous identification of möbius aromaticity for meso-aryl-substituted [28]hexaphyrins(1.1.1.1.1.1). *J. Am. Chem. Soc.* **2008**, *130*, 13568–13579.
- (33) Torrent-Sucarrat, M.; Navarro, S.; Cossío, F. P.; Anglada, J. M.; Luis, J. M. Relevance of the DFT method to study expanded porphyrins with different topologies. *J. Comput. Chem.* **2017**, *38*, 2819–2828.
- (34) Bauer, B.; Bravyi, S.; Motta, M.; Chan, G. K.-L. Quantum algorithms for quantum chemistry and quantum materials science. *Chem. Rev.* **2020**, *120*, 12685–12717.
- (35) Li, W.; Huang, Z.; Cao, C.; Huang, Y.; Shuai, Z.; Sun, X.; Sun, J.; Yuan, X.; Lv, D. Toward practical quantum embedding simulation of realistic chemical systems on near-term quantum computers. *Chem. Sci.* **2022**, *13*, 8953–8962.
- (36) Barkoutsos, P. K.; Gonthier, J. F.; Sokolov, I.; Moll, N.; Salis, G.; Fuhrer, A.; Ganzhorn, M.; Egger, D. J.; Troyer, M.; Mezzacapo, A.; et al. Quantum algorithms for electronic structure calculations: Particle-hole hamiltonian and optimized wave-function expansions. *Phys. Rev. A* **2018**, *98*, No. 022322.
- (37) Peruzzo, A.; McClean, J.; Shadbolt, P.; Yung, M.-H.; Zhou, X.-Q.; Love, P. J.; Aspuru-Guzik, A.; O'Brien, J. L. A variational eigenvalue solver on a photonic quantum processor. *Nat. Commun.* **2014**, *5*, 4213.
- (38) Steiner, E.; Fowler, P. W. On the orbital analysis of magnetic properties. *Phys. Chem. Chem. Phys.* **2004**, *6*, 261–272.
- (39) Steiner, E.; Fowler, P. W. Four- and two-electron rules for diatropic and paratropic ring currents in monocyclic π systems. *Chem. Commun.* **2001**, 2220–2221.

- (40) Steiner, E.; Fowler, P. W. Patterns of ring currents in conjugated molecules: A few-electron model based on orbital contributions. *J. Phys. Chem. A* **2001**, *105*, 9553–9562.
- (41) Wentholt, P. G.; Hrovat, D. A.; Borden, W. T.; Lineberger, W. C. Transition-state spectroscopy of cyclooctatetraene. *Science* **1996**, *272*, 1456–1459.
- (42) Karadakov, P. B.; Gerratt, J.; Cooper, D. L.; Raimondi, M. The electronic structure of cyclooctatetraene and the modern valence-bond understanding of antiaromaticity. *J. Phys. Chem.* **1995**, *99*, 10186–10195.
- (43) Baird, N. C. Quantum organic photochemistry. II. Resonance and aromaticity in the lowest 3.Pi.Pi.* state of cyclic hydrocarbons. *J. Am. Chem. Soc.* **1972**, *94*, 4941–4948.
- (44) Rosenberg, M.; Dahlstrand, C.; Kilså, K.; Ottosson, H. Excited state aromaticity and antiaromaticity: Opportunities for photophysical and photochemical rationalizations. *Chem. Rev.* **2014**, *114*, 5379–5425.
- (45) Karadakov, P. B. Norcorrole: Aromaticity and antiaromaticity in contest. *Org. Lett.* **2020**, *22*, 8676–8680.
- (46) Bean, D. E.; Fowler, P. W.; Soncini, A. Double aromaticity and ring currents in open-shell systems. *Chem. Phys. Lett.* **2009**, *483*, 193–197.
- (47) Heilbronner, E. Why do some molecules have symmetry different from that expected? *J. Chem. Educ.* **1989**, *66*, 471–478.
- (48) Stanger, A. The different aromatic characters of some localized benzene derivatives. *J. Phys. Chem. A* **2008**, *112*, 12849–12854.
- (49) Soncini, A.; Domene, C.; Engelberts, J. J.; Fowler, P. W.; Rassat, A.; van Lenthe, J. H.; Havenith, R. W. A.; Jenneskens, L. W. A unified orbital model of delocalised and localised currents in monocycles, from annulenes to azabora-heterocycles. *Chem.—Eur. J.* **2005**, *11*, 1257–1266.
- (50) Monino, E.; Boggio-Pasqua, M.; Scemama, A.; Jacquemin, D.; Loos, P.-F. Reference energies for cyclobutadiene: Automerization and excited states. *J. Phys. Chem. A* **2022**, *126*, 4664–4679.
- (51) Shaik, S.; Shurki, A.; Danovich, D.; Hiberty, P. C. A different story of π -delocalization—the distortivity of π -electrons and its chemical manifestations. *Chem. Rev.* **2001**, *101*, 1501–1540.
- (52) Binsch, G.; Heilbronner, E.; Murrell, J. N. The theory of double bond fixation in conjugated hydrocarbons. *Mol. Phys.* **1966**, *11*, 305–320.
- (53) Fowler, P. W. Symmetry aspects of distortivity in π systems. In *Adv. Quantum chem.*, Vol. 44; Academic Press, 2003; pp 219–237
DOI: [10.1016/S0065-3276\(03\)44014-8](https://doi.org/10.1016/S0065-3276(03)44014-8).
- (54) Fowler, P. W.; Rassat, A. Symmetry and distortive π -electrons in two- and three-dimensional conjugated systems. *Phys. Chem. Chem. Phys.* **2002**, *4*, 1105–1113.
- (55) Angeli, C.; Borini, S.; Cestari, M.; Cimiraglia, R. A quasidegenerate formulation of the second order n-electron valence state perturbation theory approach. *J. Chem. Phys.* **2004**, *121*, 4043–4049.
- (56) Fowler, P. W.; Mizoguchi, N.; Bean, D. E.; Havenith, R. W. A. Double aromaticity and ring currents in all-carbon rings. *Chem.—Eur. J.* **2009**, *15*, 6964–6972.
- (57) Soncini, A.; Teale, A. M.; Helgaker, T.; De Proft, F.; Tozer, D. J. Maps of current density using density-functional methods. *J. Chem. Phys.* **2008**, *129*, No. 074101.
- (58) Havenith, R. W. A.; Meijer, A. J. H. M.; Irving, B. J.; Fowler, P. W. Comparison of ring currents evaluated consistently at density functional and Hartree–Fock levels. *Mol. Phys.* **2009**, *107*, 2591–2600.
- (59) Sokolov, I. O.; Barkoutsos, P. K.; Ollitrault, P. J.; Greenberg, D.; Rice, J.; Pistoia, M.; Tavernelli, I. Quantum orbital-optimized unitary coupled cluster methods in the strongly correlated regime: Can quantum algorithms outperform their classical equivalents? *J. Chem. Phys.* **2020**, *152*, 124107.
- (60) Zhang, R.; Ellern, A.; Winter, A. H. Anti-aromaticity relief as an approach to stabilize free radicals. *Angew. Chem., Int. Ed.* **2021**, *60*, 25082–25088.